AIAA JOURNAL
Vol. 34, No. 10, October 1996

# Elastic Wave Generation by Piezoceramic Patches

Mohammad A. Moetakef,* Shiv P. Joshi,† and Kent L. Lawrence‡
*University of Texas at Arlington, Arlington, Texas 76019-0018*

**Elastic flexural and longitudinal waves can be generated in structure by using piezoelectric transducers. These waves may be used to obtain fundamental properties of the medium or to locate flaws. Bulk waves can be created in a thin piezoelectric plate by applying an electrical signal to interdigital electrodes deposited on each side of the plate. These transducers can be used to generate ultrasonic bulk waves with a wide range of frequencies and amplitudes controlled by a number of electrodes and a delayed voltage independently applied to each electrode. Numerical results demonstrating the finite element simulation of piezoelectric actuators and sensors in generating and detecting elastic bulk waves are presented. Experimental observations of flexural waves generated by surface mounted piezoceramic plates are compared with the finite element results. Bulk wave generation and detection using interdigital electrodes are simulated and their potential application as probes in smart structures is discussed.**

## I. Introduction

IN some nondestructive examination (NDE) techniques, elastic waves are used to determine fundamental properties of the materials or to detect localized damage in the structure. In signal processing, bulk waves and surface acoustic waves (SAW) are used in ultrasonic delay lines and SAW devices. Bulk waves are basically characterized by two modal types of mechanical excitation, that is, longitudinal or compressional waves and transverse or shear waves. The primary means for generating or detecting waves in these applications are piezoelectric transducers. Surface-mounted piezoelectric actuators or sensors are the most common elements used to generate and detect elastic waves. These actuators operate based on the principle of electric-field-induced strain. Depending on the type of driving electric field, i.e., dc, ac, or pulse, rigid displacement, vibrating strain, or transient waves can be developed.

Recent interest in developing smart structures has created new demands for employing novel NDE techniques as an integral part of the structure. Damage detection in a structure with desirable resolution can be done by mapping the entire structure. For damage mapping, three types of pulses, constant frequency (CF), frequency modulated (FM), and combined CF-FM, can be generated by piezoelectric transducers. A long CF pulse is appropriate for detecting cracks larger than the wavelength of the signal; this pulse, however, is not suitable for locating a target precisely or extricating its detail. To obtain more information about the target features, a large number of frequencies are needed. FM bursts contain more time information, which may be used to compute echo delays and, hence, to determine the distance to a target. The combined CF-FM pulses can be observed in nature in the signals emitted by the mustached bat. These signals consist of a long CF component followed by a short FM burst.[1] Interdigital (ID) transducers, widely used in SAW devices, can be employed to generate and to detect ultrasonic bulk waves. By means of these transducers, it is possible to generate highly amplified pulses that can be employed in conjunction with beam steering techniques to probe the interior of an object for damage mapping.[2] The flexibility in the periodic arrangement of these electrodes makes generation of various types of pulses and thereby damage mapping possible.

The numerical modeling of transient wave propagation has recently attracted attention from investigators. Harumi[3] conducted computer simulation of ultrasonics in solids for the purpose of NDE. Sansalone et al.[4] studied transient wave propagation by using the finite element method. Developments in the finite element simulation of waves launched by piezoelectric transducers is rather recent in origin. Ostergaard and Pawlak[5] reviewed the three-dimensional formulation of finite elements coupled with electroelastic equations of motion and compared the computational results for calculated mode shapes, natural frequencies, and frequency response curves of ultrasonic transducers with experimental data. Friedrich et al.[6] applied the finite element method to simulate piezoelectric Lamb wave delay lines and thereby to compute the electrical impulse response of the device. The simulation involved a thin piezoelectric plate with symmetric electrode structures on both sides of the plate. Lerch[7] performed simulation of piezoelectric media to obtain the natural frequencies and related eigenmodes of piezoelectric sensors and actuators.

To develop ID transducers, it is helpful to use computer simulation to predict the characteristics of a given design. Because of the versatility of this numerical technique, complex geometries and material properties associated with practical test situations can be easily modeled. Additionally, different periodic arrangements of ID electrodes in bulk elastic wave devices can be simulated by the finite element method, which helps in planning of appropriate NDE procedures for configurations with sensors/actuators as an integral part of the structure.

In the present work, a linear strain tetrahedral finite element along with a Newmark–Wilson time integration scheme has been employed to perform numerical simulation of elastic bulk waves generated by piezoelectric transducers. A detailed finite element formulation is presented in Ref. 8. Both finite element simulations of flexural waves generated by surface-mounted piezoelectric plates and longitudinal waves generated by ID transducers have been studied. To show the accuracy of the computer simulation, the numerical outputs of the first case have been compared with experimental observations. Frequency and amplitude-controlled ultrasonic signals generated by ID transducers have also been discussed. The potential application of ID transducers as probes in smart structures for damage mapping has been studied as well.

## II. Bulk Wave Generation

By mounting piezoceramic plates on both sides of a beam and applying a pulse of potential difference, longitudinal or flexural waves are produced in the beam. The type of generated waves depends on the direction of polarization in piezoelectric components and that of the applied voltage. Alternatively, an ID transducer may be used to create bulk waves. An ID transducer consists of an array of electrodes or fingers connected alternately to two bus-bars and deposited on a piezoelectric substrate (Fig. 1). These transducers are used extensively in ultrasonic delay lines and SAW devices to generate or detect surface waves. When an oscillatory potential difference is applied to the electrodes, the transducer generates an electric field

Received June 29, 1995; revision received April 15, 1996; accepted for publication April 16, 1996. 

*Graduate Student, Department of Mechanical and Aerospace Engineering; currently Project Engineer, Automated Analysis Corporation, 2805 S. Industrial Road, Suite 100, Ann Arbor, MI 48104.

†Associate Professor, Department of Mechanical and Aerospace Engineering. Member AIAA.

‡Professor, Department of Mechanical and Aerospace Engineering.

that is spatially periodic with its period, $2\Lambda$, equal to the spacing of electrodes connected to one of the bus-bars. The developed electric field, in turn, induces strains in the vicinity of the piezoelectric surface leading to the generation of elastic waves. In surface wave propagation, only a small depth of material (on the order of the wavelength) is disturbed. For an applied impulse type voltage, when the electrode spacing in an ID transmitter is equal to or close to the wavelength $\Lambda$ of the wave, all mechanical disturbances interfere constructively. This requires an appropriate frequency for the applied potential difference. Figure 1 illustrates this correlation. In the case of an alternating pulse type voltage, to have a constructive interference, the electrodes spacing must be $\Lambda/2$ and the electrode width should be $\Lambda/4$. Electrical output signals in an ID receiver can also be manipulated by a proper arrangement of the array of electrodes.

In addition to surface waves, ID transducers used in SAW devices can generate bulk waves. These waves are usually detrimental to the performance of such devices, and their presence is highly undesirable.[9] By applying an electrical signal to ID electrodes deposited on both sides of a thin piezoelectric plate bulk, waves can be created. In such a device, called a cross-field type in contrast to an in-line type of SAW device, electric fields are normal to the surface of the piezoelectric plate and perpendicular to the wave propagation path. To generate in-phase bulk waves by a cross-field interdigital (CFID) transducer, the same coordination between the operating frequency and the electrode spacing as in in-line transducers must occur. To reduce the radiated bulk waves that are not in the direction

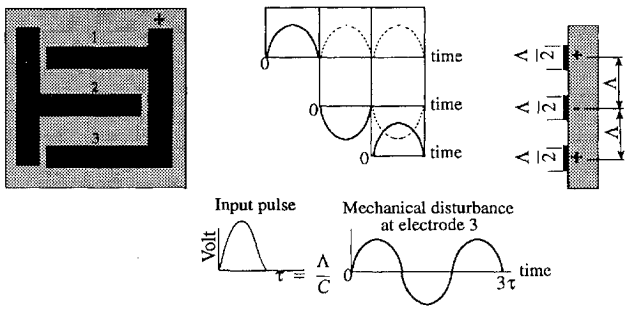


**Fig. 1 Pulse response of a three-fingered ID transducer.**

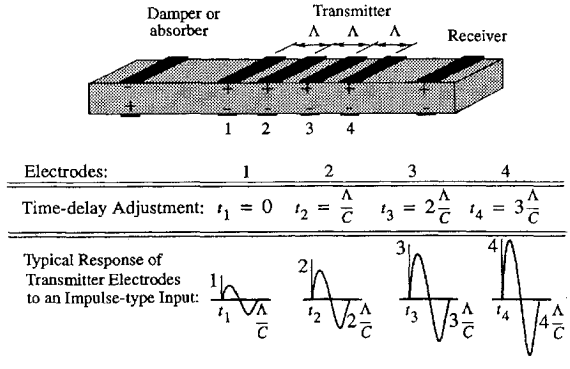


**Fig. 2 Time delay adjustment in CFID transducer and amplitude amplification of generated longitudinal bulk wave.**

orthogonal to the electric field and thus reduce reflected waves, the piezoelectric plate is required to be thin.

The CFID transducer can be used to generate ultrasonic bulk waves with a wide range of frequencies. The amplitude of the wave can be controlled by the number of the electrodes and a delayed voltage independently applied to each electrode. The delay time, which is determined by the wave velocity in the piezoelectric plate and desired wavelength (or electrodes spacing), can be achieved by an electronically controllable delay line. The wave propagation is bidirectional, and therefore in SAW devices, wax absorbers are usually used to suppress the wave transmissions in one direction. In the case of CFID transducers, a pair of electrodes with opposite electric fields can perform the task of wave suppression. The time delay adjustment for the damper needs to be based on its location and the time delay of each transmitter electrode. The receiver electrodes, which convert mechanical disturbances to output voltages, can also have an array-type arrangement for the manipulation of the output signals. The basic principles of operation for a typical CFID transducer are illustrated in Fig. 2.

By polarizing the piezoelectric plate in the appropriate direction, different types of waves (longitudinal, flexural, and torsional waves) can be generated. However, in the case of dispersive waves, CFID transducers do not have the desired performance. This is because of the concurrence of the time delay required for establishing an electric field to an electrode and the time that it takes the wave to reach the same electrode. Nevertheless, it should be noticed that the most important types of waves for industrial ultrasonic applications are longitudinal and shear waves, which are both nondispersive.

Because CFID transducers do not operate at their fundamental frequency, a certain thickness for resonance is not necessary. However, to reduce wave reflections, a thin piezoelectric plate is required. For beam steering, several CFID transducers can be laminated together. Each lamina may have a different overall time delay, which can be set in such a way that wave fronts with a higher intensity in a certain direction, e.g., normal, angled, or focused, can be generated.[2] Owing to the flexibility of the electrodes arrangement, laminated CFID transducers provide a flexible technique for beam steering.

A CFID transducer can be used as an external probing device in conventional NDE procedures. Because of its compactness and its capability for beam steering, it also can be used as a damage detection constituent in a smart structure. In this application, the transducer remains fixed within the structure, and through electronic beam steering, the entire structure is mapped for damage detection.[10]

## III. Experimental Setup and Apparatus

An experimental setup as shown in Fig. 3 is used to generate the flexural wave in a 6061-T6 aluminum beam. The beam is clamped at one end. At the free end, piezoceramic plates of lead zirconate titanate, PZT-850, are mounted on both sides of the beam. Table 1 shows the material properties for aluminum and PZT-2 (PZT-850 is equvivalent to the standard PZT-2 according to American Piezoceramics, Inc.). The electroded surfaces of the piezoceramic plates are bonded to brass strip terminals by cold solder Eccobond 57C. Cold soldering is required to prevent possible damage from hot soldering to the piezoceramic and its polarity. To ensure effective conversion of electrical energy of the piezoceramic plates to the mechanical energy in the substrate beam, one of the stiffest available epoxies, Depend II, is used to bond the PZT plates to the beam.

**Table 1 Material properties for PZT-2 and aluminum**

| | Elastic compliance, $m^2/N$ | Piezoelectric voltage coeff., $m^2/C$ | Piezoelectric strain coeff., m/V | Dielectric, $N/V^2$ | Density, $kg/m^3$ |
|---|---|---|---|---|---|
| PZT-2 | $S_{11}^E$: $11.6 \times 10^{-12}$ | $g_{31}$: $-15.1 \times 10^{-3}$ | $d_{31}$: $-60.2 \times 10^{-12}$ | $\varepsilon_{11}$: $4.46 \times 10^{-9}$ | $\rho$: 7600 |
| | $S_{22}^E$: $-3.33 \times 10^{-12}$ | $g_{33}$: $38.1 \times 10^{-3}$ | $d_{33}$: $152 \times 10^{-12}$ | $\varepsilon_{33}$: $2.3 \times 10^{-9}$ | — |
| | $S_{13}^E$: $-4.97 \times 10^{-12}$ | $g_{15}$: $50.3 \times 10^{-3}$ | $d_{15}$: $440 \times 10^{-12}$ | — | — |
| | $S_{33}^E$: $14.8 \times 10^{-12}$ | — | — | — | — |
| | $S_{44}^E$: $45.0 \times 10^{-12}$ | — | — | — | — |
| | $S_{66}^E$: $29.9 \times 10^{-12}$ | — | — | — | — |
| Al-6061 | $S_{11}$: $14.5 \times 10^{-12}$ | — | — | — | — |
| | $S_{12}$: $-4.74 \times 10^{-12}$ | — | — | — | — |

The equipment used for generating and triggering the pulse signals includes a Hewlett–Packard 3245A universal source and a Hewlett–Packard 3325B synthesizer/function generator. The Trek 50/750 high-voltage power supply amplifies the generated pulse before being applied to the piezoceramic plates.

Data acquisition is achieved by a fiber-optic laser interferometer (Polytec OFV 1000) that measures the voltage proportional to the transverse velocity of any desired point on the surface. A digital oscilloscope (Norland Prowler) is used to display the output signal from the laser interferometer and to transfer these signals (in ASCII format) to the storage device of a computer. Because of the memory restriction, every eighth data point is collected by the storage device.

## IV. Finite Element Modeling

### Surface-Mounted PZT Transducer

Figure 4 shows the physical and the finite element models of the beam. Dimensions of each model are summarized in Table 2. The finite element model consists of 1200 LST (linear strain tetrahedral) elements and 4071 nodes. Because of the symmetry about $x$–$y$ and $x$–$z$ planes, only one quarter of the beam is modeled. Additionally, since the input signal generates disturbance in the form of plane waves perpendicular to the direction of propagation, in the numerical analysis a one-element model in the $y$ direction is sufficient. For time integration, the Newmark–Wilson method with 500 time steps of 2 $\mu$s is used. This time step size has been found to be small enough to produce negligible numerical damping.

**Table 2 Dimensions of aluminum beam and piezoceramic plate**

| | | Length, mm | Width, mm | Height, mm |
|---|---|---|---|---|
| Physical model | Aluminum beam | 1500 | 25.4 | 3.175 |
| | PZT plates | 25.4 | 25.4 | 1.3716 |
| Finite element model | Aluminum beam | 1498.6 | 1.5876 | 1.5876 |
| | PZT plates | 25.4 | 1.5876 | 1.3716 |

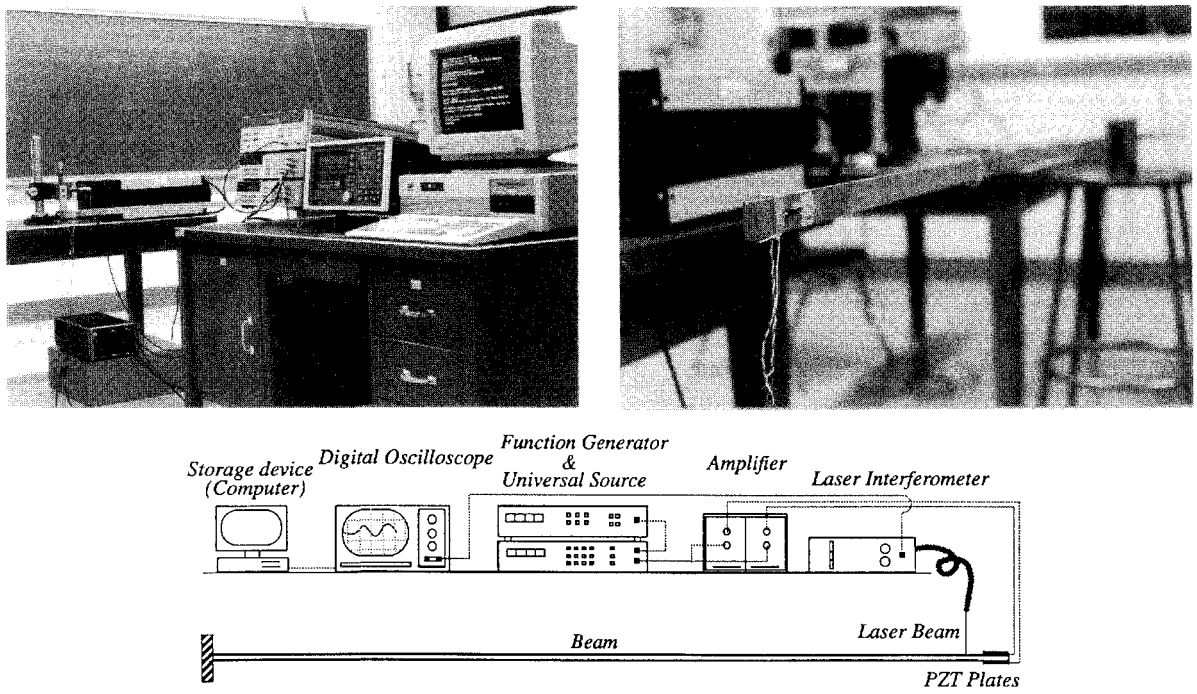


**Fig. 3 Experimental arrangement: photograph and block diagram.**

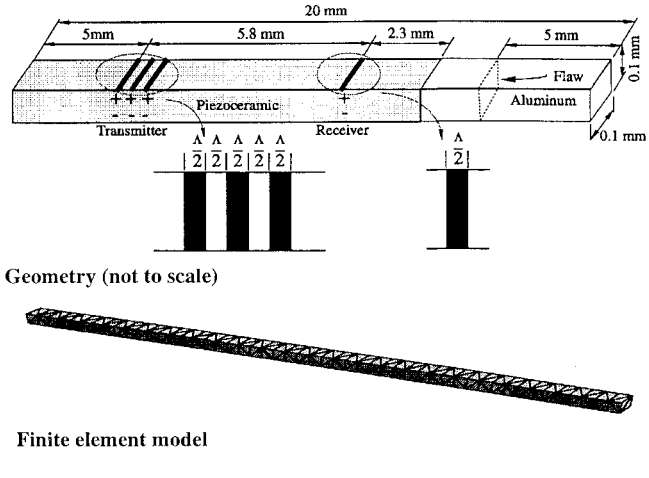


**Fig. 4 Physical and finite element model of the beam. Number of elements: 1000 LST; number of nodes: 3409; dimensions: 20 × 0.05 × 0.05 mm; time step size: 0.01 $\mu$s; and pulse duration: 0.215 $\mu$s ($\Lambda$ = 0.8 mm) and 0.430 $\mu$s ($\Lambda$ = 1.6 mm).**

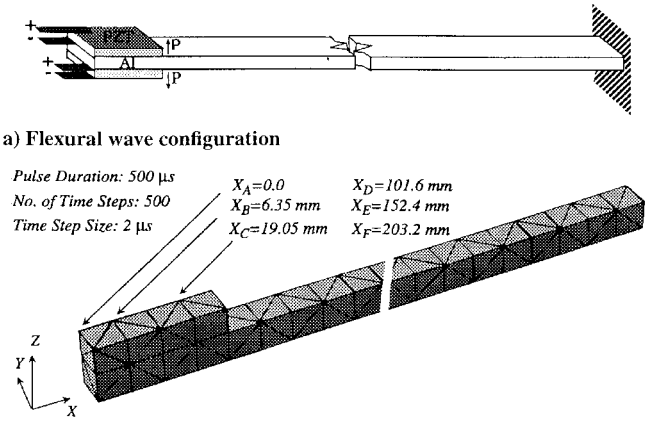


**Fig. 5 Geometry and finite element model of transducer.**

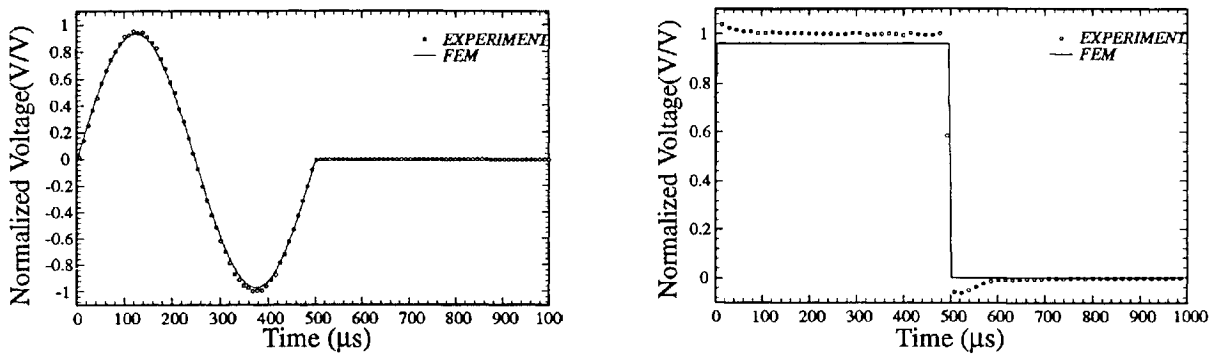


Sinusodial pulse Square pulse

Fig. 6 Experimental input pulses and their numerical approximations.

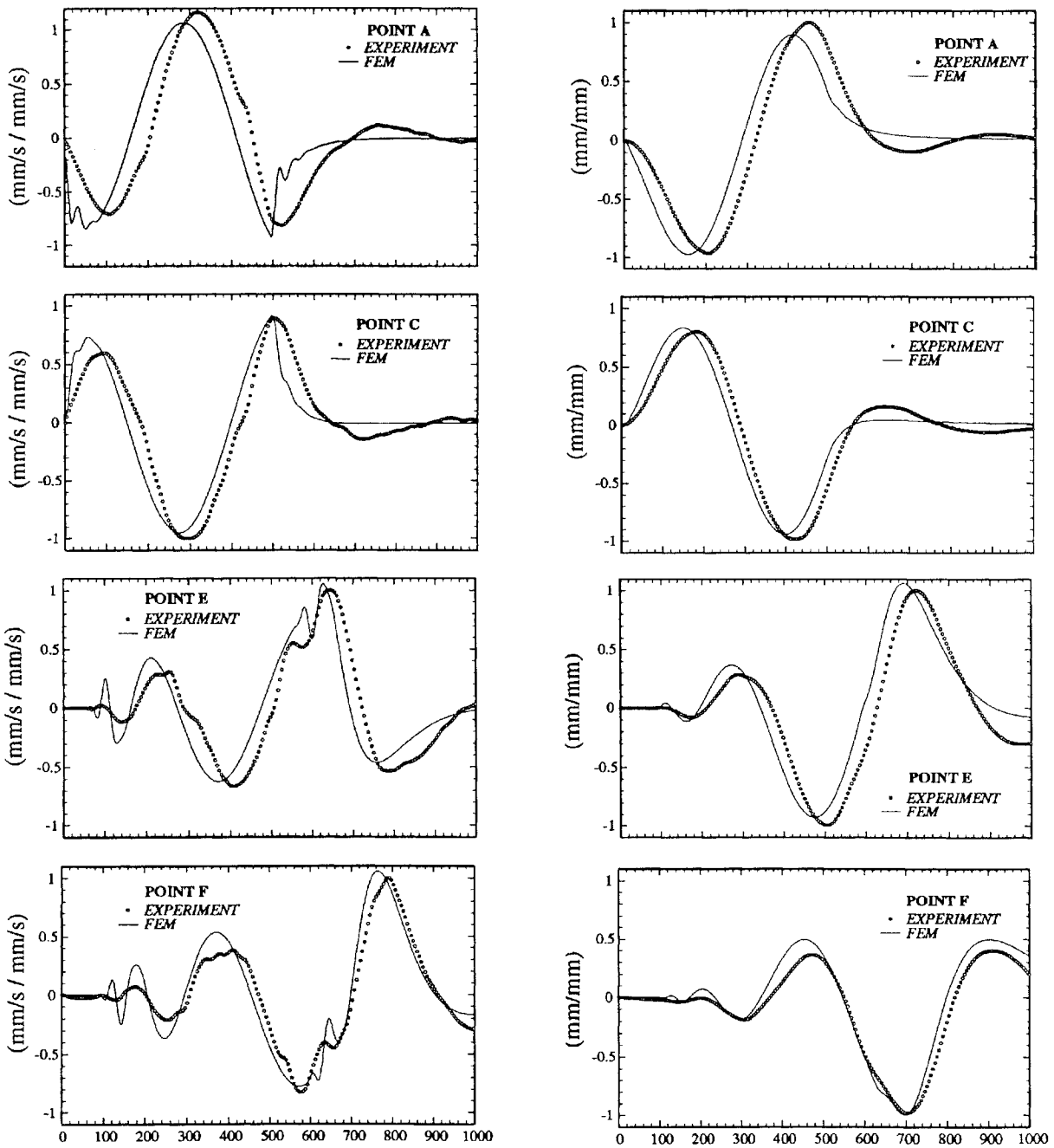


Normalized transverse velocity Normalized transverse displacement

Fig. 7 Time history of transverse velocity and displacement for a pulse of single sine wave.

**CFID Transducer**

The finite element model involves the generation of bulk longitudinal waves by an array of transmitter electrodes. The CFID transducer is fixed to an aluminum beam that contains an artificial defect. The incident and reflected waves are sensed by a pair of receiver electrodes. PZT-8 is used in the numerical simulation of CFID because it has a higher piezoelectric coefficient than PZT-2. Material properties for the aluminum and piezoceramic, given in Table 3, are utilized in the numerical simulation. Because of symmetry, only one quarter of the transducer and the beam is modeled by a mesh with 1000 LST finite elements (see Fig. 5). Potential differences of 1 V in the form of a pulse of half a sine wave with appropriate time delay are established across the thickness of the PZT at the transmitter electrodes.

To simulate a cavity in the aluminum beam, the material properties in the region of the cavity were made 100,000 times smaller than the material properties of the surrounding aluminum. Figure 5a shows the location of the flaw. The analysis is presented for various numbers of electrodes and for wavelengths of 0.8 and 1.6 mm.

## V. Results and Discussion

The experiment and analysis are conducted for two different input signals, that is, a single sinusoidal wave and a square pulse. Each case holds a pulse duration of 500 $\mu$s and an amplitude of 250 V. The input pulses result in a potential difference of 500 V across the thickness of each piezoceramic plate. The input in finite element analysis is in the form of nodal charges equivalent to the supplied

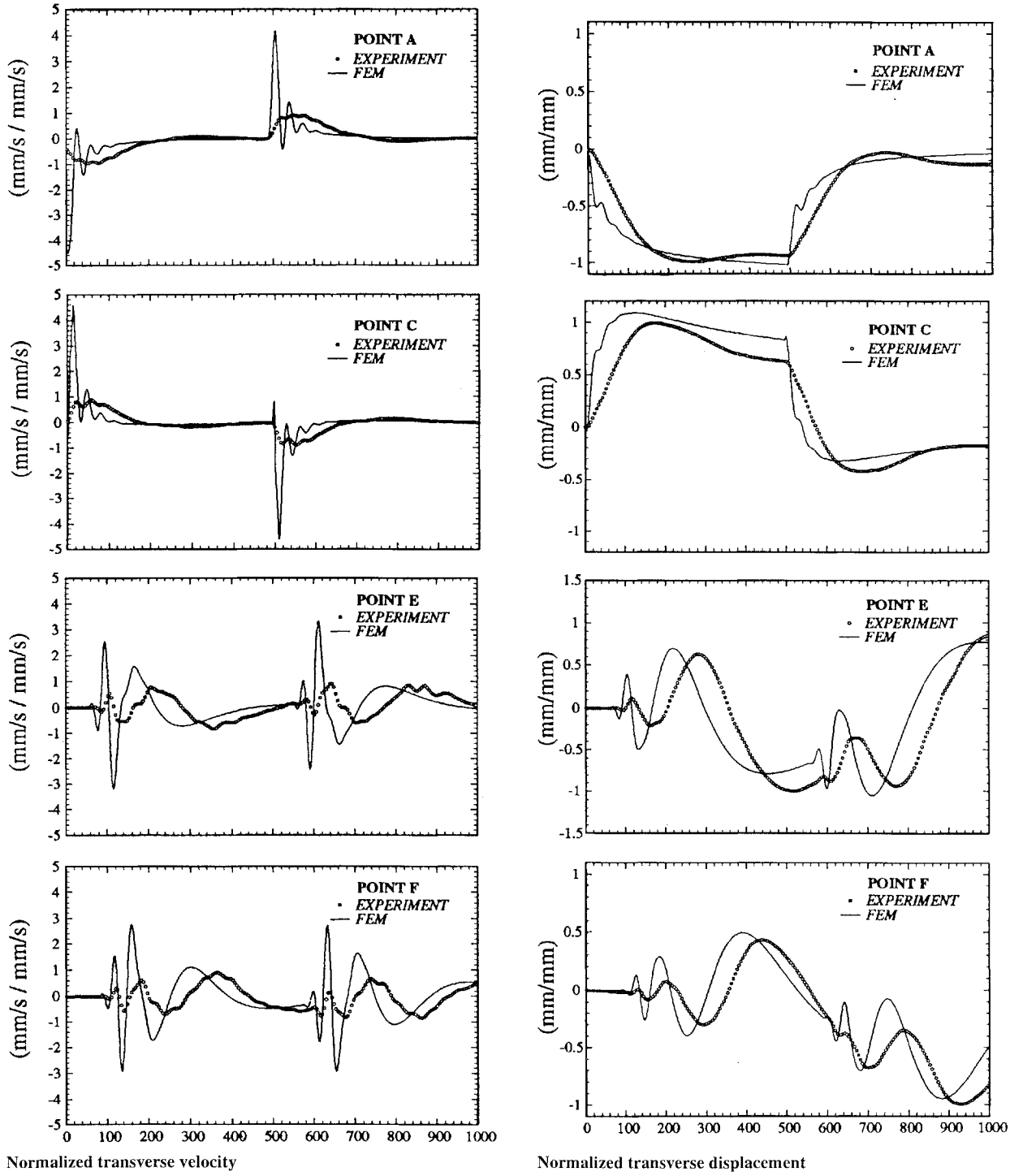


Fig. 8 Time history of transverse velocity and displacement for a pulse of square wave.

**Table 3 Material properties for PZT-8**

| | Elastic compliance, $m^2/N$ | Piezoelectric voltage coeff., $m^2/C$ | Piezoelectric strain coeff., m/V | Dielectric, $N/V^2$ | Density, $kg/m^3$ |
|---|---|---|---|---|---|
| PZT-8 | $S_{11}^E$: $11.5 \times 10^{-12}$ | $g_{31}$: $-10.9 \times 10^{-3}$ | $d_{31}$: $-0.97 \times 10^{-12}$ | $\varepsilon_{11}$: $7.96 \times 10^{-9}$ | $\rho$: 7600 |
| | $S_{22}^E$: $-3.7 \times 10^{-12}$ | $g_{33}$: $25.4 \times 10^{-3}$ | $d_{33}$: $225 \times 10^{-12}$ | $\varepsilon_{33}$: $5.31 \times 10^{-9}$ | — |
| | $S_{13}^E$: $-4.8 \times 10^{-12}$ | $g_{15}$: $28.9 \times 10^{-3}$ | $d_{15}$: $330 \times 10^{-12}$ | — | — |
| | $S_{33}^E$: $13.5 \times 10^{-12}$ | — | — | — | — |
| | $S_{44}^E$: $31.9 \times 10^{-12}$ | — | — | — | — |
| | $S_{66}^E$: $30.4 \times 10^{-12}$ | — | — | — | — |

voltage. These charges are obtained from a static analysis with the desired potential difference (voltage) as input.

Figure 6 shows the input pulses along with their numerical approximations. The experimental data represent the voltage applied to each electroded surface of the PZT plates. The numerical plots, which are for point A (Fig. 5), are the results of input nodal charges equivalent to the experimentally applied voltage. The plots are normalized with respect to the absolute maximum of the experimental input. It can be seen that input signals in the experiment are closely approximated by the numerical output voltage. All experimental data are reduced and least-square smoothed. This data reduction is in addition to the one that is the result of memory restrictions in the computer storage device.

Time histories of the transverse velocity and displacement for the inputs of single sine and square pulses are shown in Figs. 7 and 8, respectively. The checkpoints include two positions (A and C) on the piezoceramic plate and another two on the aluminum substrate (E and F). Each curve was first normalized using its maximum amplitude. Calculated data were then normalized using the maximum value of the corresponding experimental results (see Appendix A). The experimental results for the velocity are numerically integrated to obtain the displacement profiles.

The velocity and displacement profiles for the positions located on the piezoelectric plate indicate that all of the piezoceramics points experience simultaneous deformation. Furthermore, it can be noticed that the profiles for points A and C are inverted. The dispersive wave propagation in the aluminum substrate and delayed response for the far-field points can be observed from the time history plots. The velocity–time profile for points E and F clearly shows the excitation of high frequencies as a result of the leading and trailing edges of the input pulses. The excitation appears at two different times with a time delay almost equal to the input pulse duration. Because of the sharper gradient change, the high-frequency excitation is more apparent for the case of a square pulse input.

The results from the finite element analysis, compared with those from the experiment, exhibit steeper and quicker response. In addition, according to the velocity and displacement profiles for points E and F, the disturbance propagates faster in the finite element model than in the physical one. The higher wave speed is attributed to the higher stiffness of the finite element model because of the limited number of degrees of freedom. Appendix B demonstrates the effect of mesh refinement (the number of elements used in the current numerical analysis has been found to be efficient, and the contribution of a more refined mesh to the improvement of the results has turned out to be insignificant).

Note that the velocity measurements in the experimental model by laser interferometer are position measurements at some points on the surface. The experimental measurement, therefore, involves two components, one resulting from the transverse motion of the points and one resulting from the deformation or strain that occurred at that position. In contrast, the velocities obtained by finite element analysis only involve the former component of the experimental measurements. Briefly, the experimental measurement provides Lagrangian information, whereas the numerical analysis yields Eulerian output. Since through numerical analysis enough information in Eulerian form is available, it is possible to derive numerical data in Lagrangian terms. It can be shown, however, that the difference between transverse velocity in Lagrangian and Eulerian terms is on the order of the strain.[11] Considering the very large magnitude of transverse velocity in comparison with the strain, it is realized that

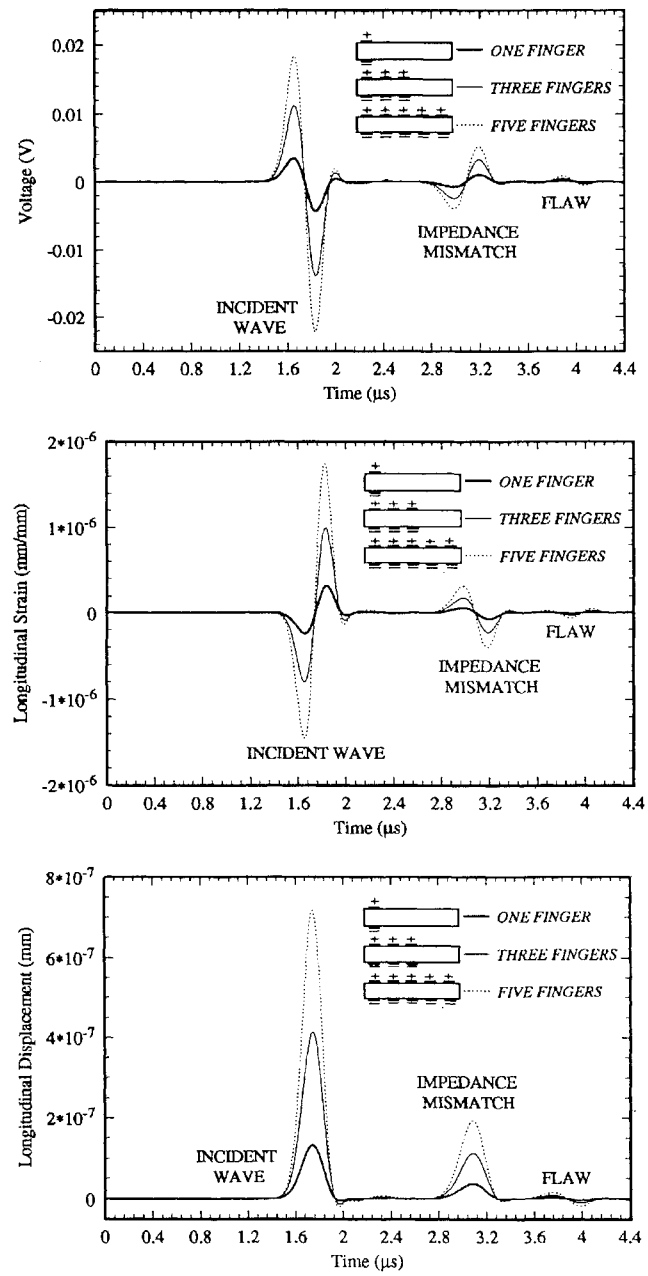


**Fig. 9 Output voltage, longitudinal strain, and displacement at the receiver for different number of electrodes.**

the aforementioned difference is trivial. Therefore, comparing the velocities in numerical Eulerian form with those measured experimentally does not introduce significant errors.

The mathematical model in the finite element analysis represents an ideal model with a perfect and immediate bond between the piezoceramic plates and the aluminum beam, thus, neglecting the entity of adhesive epoxy. The model, additionally, ignores any physical

source of energy dissipation or response retardation that leads to damping or hysteresis. Ignoring such kinds of effects and invoking simplifications in the mathematical model, in addition to the numerical errors originating from the spatial and temporal discretization of the model, lead to differences between the experimental and numerical results. This discrepancy in the results is more significant in the case of square pulse input, which, as mentioned before, is a result of the sharper gradient change and the overshoot arising from the numerical time integration, a behavior similar to the Gibbs phenomena.[12] However, the finite element output, especially the lower-frequency waves, is in overall good agreement with the experiment.

Only numerical simulations of elastic waves generated by a CFID transducer are presented. From Fig. 9 it can be seen that increasing the number of electrodes amplifies the output signals. The amplification is proportional to the number of electrodes. An impedance mismatch at the interface of the PZT transducer and the aluminum beam leads to the reflection of the incident energy; therefore, only some percentage of the incident energy is transmitted to the aluminum beam. Similarly, the wave sensed by the receiver is only part of the wave reflected at the flaw.

## VI. Conclusion

Numerical simulation of elastic waves in a beam generated by surface-mounted piezoelectric plates has been presented. Considering the dispersive feature of flexural waves, excellent qualitative agreement between the numerical output and the experimental data has shown that the finite element simulation can be utilized for designing a CFID system.

Frequency and amplitude-controlled ultrasonic signals generated by CFID transducers have been discussed. The potential application of CFID transducers for damage detection in a structure and electronic beam steering to map the interior of the structure has been studied. To demonstrate the feasibility of using CFID transducers for the generation of frequency and amplitude-controlled bulk waves, the behavior of a CFID system has been simulated using the finite element method.

## Appendix A: Nonnormalized Experimental and Numerical Results for the Flexural Waves

Nonnormalized experimental and numerical results for the flexural waves are plotted in Fig. A1. Although the results obtained from the experiment and the finite element analysis are qualitatively in good agreement, quantitatively they are different. The major cause of this dissimilarity is the lack of accurate material properties for the physical model. The piezoelectric and elastic data provided by the manufacturer of the PZT-2 piezoceramic plates are different from those of standard PZT-2. Finite element analysis with the manufacturer's data shows significant quantitative discrepancy with experimental results. Thus, the numerical results presented throughout are based on the material properties for standard PZT-2 as given in Table 1. The manufacturer's piezoelectric and elastic data are summarized in Table A1 for reference but are not used in the numerical simulations.

Note that an important parameter in the characterization of piezoceramics is the $d_{33}$ coefficient, which expresses the ratio of the strain developed in a piezoceramic to the applied electric field. Identical piezoceramics often differ in terms of degree of poling and compositional homogeneity, which greatly affects the $d_{33}$ coefficient. The difference between experiment and calculated results is attributed to this coefficient.

## Appendix B: Effect of Mesh Refinement on the Velocity of Wave Propagation

When a physical model is spatially discretized by finite elements, the finite element model exhibits a higher than actual stiffness because of the limited number of degrees of freedom. By increasing the number of elements, the model becomes more flexible. The higher than actual frequencies are excited by a pulse-type loading. Because of the dispersive nature of the flexural wave, high-frequency waves propagate with a velocity higher than the actual velocity. As a result, refinement of the mesh in a finite element model of flexural wave problems not only affects the amplitude of the waveforms but also reduces the propagation velocity of the waves (Fig. B1).

**Table A1 Properties for PZT-850**

| Elastic compliance, $m^2/N$ | Piezoelectric, $m^2/C$ | Dielectric, m/V | Density, $kg/m^3$ |
|---|---|---|---|
| $S_{11}^E$: $15.3 \times 10^{-12}$ | $g_{31}$: $-12.4 \times 10^{-3}$ | $d_{31}$: $-175 \times 10^{-12}$ | $\rho$: 7500 |
| $S_{33}^E$: $17.3 \times 10^{-12}$ | $g_{33}$: $26.0 \times 10^{-3}$ | $d_{33}$: $450 \times 10^{-12}$ | |

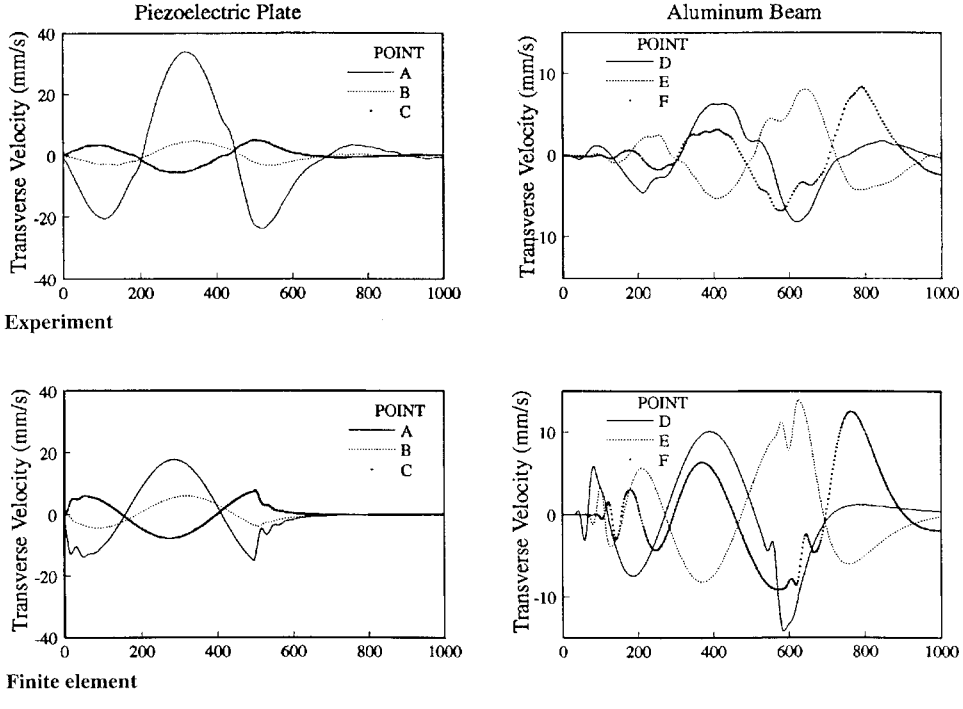


Fig. A1 Transverse velocity–time profiles at various positions.

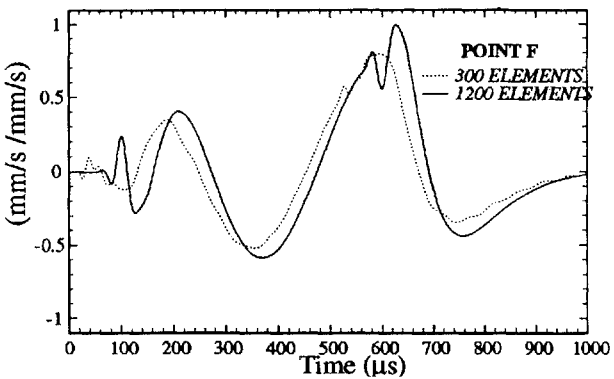


Normalized transverse velocity

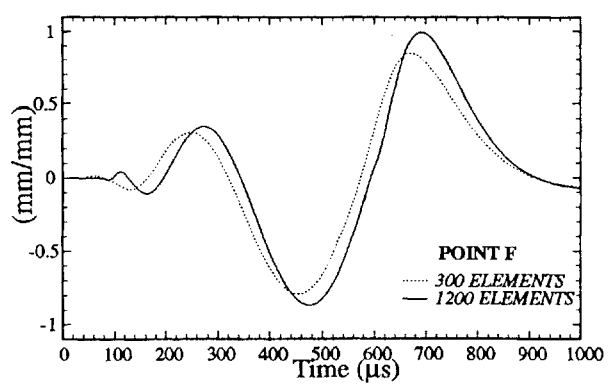


Normalized transverse displacement

**Fig. B1 Effect of mesh refinement on the speed of wave propagation.**

## References

[1]Suga, N., "Biosonar and Neural Computation in Bats," *Scientific American*, June 1990, pp. 60–68.

[2]Moetakef, M. A., Joshi, S. P., and Lawrence, K. L., "Three-Dimensional Finite Element Simulation of Bulk Elastic Waves in Piezoceramic Transducers Using Interdigital Electrodes," *Smart Structures and Materials 1995—Mathematics and Control in Smart Structures*, edited by V. V. Varadan, Vol. 2442, Society of Photo-Optical Instrumentation Engineers, Bellingham, WA, 1995, pp. 182–187.

[3]Harumi, K., "Computer Simulation of Ultrasonics in a Solid," *Materials Evaluation*, Vol. 44, Aug. 1986, pp. 1086–1114.

[4]Sansalone, M., Carino, N. J., and Hsu, N. N., "Finite Element Studies of Transient Wave Propagation," *Review of Progress in Quantitative NDT*, edited by D. O. Thompson and D. E. Chimento, Plenum, New York, 1986, pp. 125–133.

[5]Ostergaard, D. F., and Pawlak, T. P., "Three Dimensional Finite Elements for Analyzing Piezoelectric Structures," *Proceedings of IEEE Ultrasonics Symposium* (Williamsburg, VA), Inst. of Electrical and Electronics Engineers, New York, 1986, pp. 639–642.

[6]Friedrich, W., Lerch, R., Prestele, K., and Soldner, R., "Simulations of Piezoelectric Lamb Wave Delay Lines Using a Finite Element Method," *IEEE Transactions of Ultrasonics and Frequency Control*, Vol. 37, No. 2, 1990, pp. 248–253.

[7]Lerch, R., "Simulation of Piezoelectric Devices by Two- and Three-Dimensional Finite Elements," *IEEE Transactions of Ultrasonics and Frequency Control*, Vol. 37, No. 2, 1990, pp. 233–247.

[8]Moetakef, M. A., Lawrence, K. L., Joshi, S. P., and Shiakolas, P. S., "Closed Form Expressions for Higher Order Electroelastic Tetrahedral Elements," *AIAA Journal*, Vol. 33, No. 1, 1995, pp. 136–142.

[9]Campbell, C., *Surface Acoustic Wave Devices and Their Signal Processing Applications*, Academic, Boston, 1989.

[10]Joshi, S. P., and Fang, C., "Dynamic Actuation by Surface Mounted Piezoceramic Patches," *Proceedings of North American Conference on Smart Structures and Materials* (Orlando, FL), Society of Photo-Optical Instrumentation Engineers, Bellingham, WA, 1994, pp. 542–548.

[11]Moetakef, M. A., "Analysis of Structures with Piezoelectric Transducers by Three-Dimensional Finite Element Method," Ph.D. Dissertation, Mechanical Engineering Dept., Univ. of Texas at Arlington, TX, 1995.

[12]Belytschko, T., and Mullen, R., "On Dispersive Properties of Finite Element Solutions," *Modern Problems in Elastic Wave Propagation*, edited by J. Miklowitz and J. D. Achenbach, Wiley, New York, 1978.